

Fractal landscape dynamics in dense emulsions and stock prices

Clary Rodríguez-Cruz,¹ Mehdi Molaei,¹ Amruthesh Thirumalaiswamy,¹ Klebert Feitosa,² Vinothan N. Manoharan,³ Shankar Sivarajan,⁴ Daniel H. Reich,⁴ Robert A. Riggelman,¹ and John C. Crocker^{1,*}

¹*Department of Chemical and Biomolecular Engineering, University of Pennsylvania, Philadelphia, Pennsylvania*

²*Department of Physics and Astronomy, James Madison University; Harrisonburg, Virginia*

³*School of Engineering and Applied Science, Harvard University; Cambridge, Massachusetts*

⁴*Department of Physics and Astronomy, Johns Hopkins University, Baltimore, Maryland*

(Dated: October 26, 2022)

Many soft and biological materials display so-called ‘soft glassy’ dynamics; their constituents undergo anomalous random motion and intermittent cooperative rearrangements. Stock prices show qualitatively similar dynamics, whose origins also remain poorly understood. Recent simulations of a foam have revealed that such motion is due to the system evolving in a high-dimensional configuration space via energy minimization on a slowly changing, fractal energy landscape. Here we show that the salient geometrical features of such energy landscapes can be explored and quantified not only in simulation but empirically using real-world, high-dimensional data. In a mayonnaise-like dense emulsion, the experimentally observed motion of oil droplets shows that the fractal geometry of the configuration space paths and energy landscape gives rise to the anomalous random motion and cooperative rearrangements, confirming corresponding simulations in detail. Our empirical approach allows the same analyses to be applied to the component stock prices of the Standard and Poor’s 500 Index. This analysis yields remarkably similar results, revealing that stock return dynamics also appear due to prices moving on a similar, slowly evolving, high-dimensional fractal landscape.

I. INTRODUCTION

Despite the deterministic nature of classical physics, the world around us appears filled with random motion. The random Brownian motion of microscopic particles is due to ‘noise’—the collisions of molecules in incessant thermal motion [1]. The random motion of weather systems has a different origin, deterministic chaos, due to the dynamical evolution of their unstable equations of motion [2]. The random motion of foraging animals such as squirrels forms a third, distinct type of random motion, a Lévy walk, containing occasional large displacements [3]. The focus of this work is a class of systems, including foams, emulsions, pastes, and cytoskeletal structures that display strikingly similar ‘soft glassy’ dynamics [4–8], that appears distinct from the three types of random motion described above. These systems have in common strongly interacting and slowly changing constituents forming a soft solid, with structural disorder and often negligible noise, that display super-diffusive motion, non-Gaussian random displacements and intermittent cooperative motion (sometimes called ‘avalanches’). Historically, models of stock price motions have compared them variously to Brownian motion [9, 10], chaotic motion [11, 12], and Lévy processes [13], with varying degrees of success. We will claim that stock price motions more closely resemble soft glassy dynamics.

A 2016 simulation study [14] of a foam was able to reproduce the major features of soft glassy dynamics with

a strikingly simple model, and provided insights into the physical and mathematical origins of the observed phenomena. The model essentially consisted of an energy function that treated the bubbles as frictionless, compressible and polydisperse spheres. The bubbles’ positions evolved simply according to minimization of total system energy; the bubbles had no inertia, nor was any thermal noise present. Motion was triggered solely by the destabilization of energy minima due to the slow evolution of the bubble radii (mimicking Ostwald ripening). Analysis of the simulation revealed a highly complex emergent geometry for the resulting potential energy landscape, a hypersurface describing the system’s total energy spanning a high-dimensional space of all droplet coordinates. In particular, the unusual random *dynamics* of this soft glass model were closely related to the tortuous fractal *geometry* of the landscape which constrained the configuration path, with ripening’s role being only to steadily destabilize shallow energy minima to allow droplet rearrangements. For this reason, we call such motion constrained by a landscape with emergent fractal geometry *fractal landscape dynamics*.

The idea that soft glassy phenomena in general are due to fractal landscape dynamics remains essentially untested in experiment. For one, it is not obvious how to explore the geometry of an abstract high-dimensional energy landscape using imperfect and noisy empirical data. Moreover, for systems without a known interaction energy model, it is not clear how to test these ideas using simulation. Here we show how relevant features of the configuration space trajectory and energy landscape can be determined using empirical high-dimensional data such as from multiple particle tracking experiments. Ap-

* jcrocker@seas.upenn.edu

plied to an index- and density-matched dense emulsion, imaged using confocal microscopy, we find that the high-dimensional geometry closely matches the predictions of the earlier simulations. In particular, we find that the droplets' super-diffusive exponent and power-law rheology exponents are related to the configuration space path's fractal dimension, that the non-Gaussian displacements of the particles are related to the anisotropy of the path directions (and landscape 'easy' directions), and that energy minima along the path are themselves formed into fractal clusters, which give rise to the heavy-tailed amplitude distribution for cooperative rearrangements.

Our empirical approach also allows us to probe the high-dimensional landscape geometry in another system with apparent soft glassy dynamics, but which lacks a known 'energy' model—stock prices. We apply our high-dimensional analysis to the price movements of component stocks within the SP500 index, in particular the portion of those motions that is uncorrelated with the price of the index itself. Remarkably, we find very similar geometry for the high-dimensional logarithmic price path and minima clustering, only with different exponents than the emulsion case. Fractal dynamics provides an explanation for the unusual non-Gaussian distribution of stock returns, and the cooperative returns' underlying spikes in volatility. This picture suggests that the market moves continuously between transient, shallow price equilibria, while highly constrained by a competitive landscape with emergent fractal geometry.

II. EXPERIMENTAL APPROACH

While studying the shape of a fractal curve in a configuration space having hundreds of dimensions may seem daunting, we will use three readily understandable geometrical analyses, sketched in Fig. 1. In practice, we will also find that each of these geometrical features relates to one or more unexplained features of the system's dynamics. First, we will assess the path's tortuosity on different length-scales. As shown in Fig. 1a, we will consider random pairs of points on the path, and compute both the high-dimensional Euclidean distance between them, $\Delta R(t, \tau) = \|\vec{R}(t + \tau) - \vec{R}(t)\|$, and the contour distance (or path length) between them, Δs . Comparing these two distances (averaged over many pairs of points) reports how tortuous the curve is, often quantified with a fractal dimension, D_f . Second, we will consider the directions taken by the path as it meanders through space. As in Fig. 1b, by studying the angular distribution of the path directions we will determine if the directions are random (isotropic in configuration space), or restricted to a smaller range of directions, as often the case for fractal curves. Third, we will examine the clustering of the stable equilibria points that the path runs between. Specifically, as in Fig. 1c, we will measure the distribution of distances between the equilibria, $P(\Delta R)$. If the minima are clustered to form a fractal themselves,

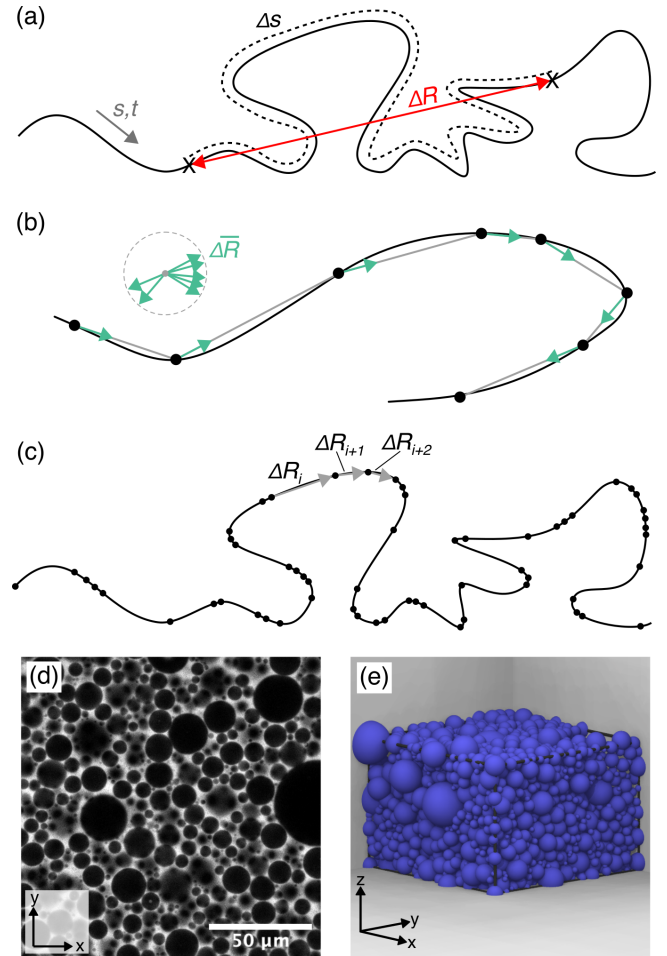


FIG. 1. Paths taken by an SGM system can be analyzed experimentally in high-dimensional space. (a) Random pairs of points on the high-dimensional path are chosen to compute their Euclidean distance, ΔR , and their contour distance, Δs . (b) Displacements between different points are converted to unit length vectors to study their angular distribution. (c) Euclidean distances between adjacent minima (dots) are measured to quantify their spatial distribution. (d) A confocal micrograph shows a section through a dense emulsion, field is $150 \mu\text{m}$ on a side. (e) A computer generated reconstruction of the same dense emulsion. Viewing volume is $145 \times 145 \times 100 \mu\text{m}^3$

the distribution will show a power-law form. Together, these measures provides a detailed fingerprint of the high-dimensional fractal geometry of the configuration space path and its minima as the system moves over the landscape.

Following the configuration of a soft glassy material through its high-dimensional configurations space requires dynamical tracking of the droplets in three dimensions. We formulated a transparent dense emulsion by making the droplets have the same index of refraction as the liquid in which they were suspended. To minimize gravity effects, we also matched the mass density of the two phases to roughly 1 part in 1000. This was achieved

by using four liquids, two non-polar ones (1-bromohexane and octane) to make up the droplets, and two polar ones (formamide and water) to form the connected phase. The droplets were stabilized with a polymeric surfactant to prevent coalescence. The emulsion was prepared using a commercial homogenizer, with the volume fraction of droplets ($\phi \approx 0.80$) slightly above the jamming threshold, giving it a mayonnaise-like consistency.

Four dimensional (xyzt) imaging of the emulsion in a sealed chamber was performed using a high-speed laser-scanning confocal microscope, imaging fluorescein dye dissolved in the connected phase. A typical image is shown in Fig. 1d. The time-dependent droplet positions and radii were determined using custom-written software [15, 16]. A reconstruction is shown in Fig. 1e. As they age, foams and dense emulsions evolve to a steady state termed dynamical scaling [17] where the shape of the droplet size distribution becomes independent of time, while the mean droplet size increases as a function of sample age. Our samples were allowed to age for 7 hours prior to data acquisition, allowing the system to reach dynamical scaling [18] (see SI Appendix, Fig. 6) and slow down to the point that the droplets' motion was easily followed. The experimental results were compared to a simulation using a previously published approach [14] based upon frictionless, compressible spheres [19–21] whose radii slowly evolve due to quasi-static ripening. See SI Appendix for further details of the experimental setup and simulation.

III. SUPER-DIFFUSION AND VISCOELASTICITY DUE TO FRACTAL PATHS.

The motion of the droplets in our dense emulsion is complex and intermittent. The droplets are nearly motionless except for abrupt motions, or avalanches, where localized collections of droplets move, typically by a fraction of a their radius, see SI Appendix, Movie 1. To quantify this motion, we will first compute the droplets mean-squared displacement (MSD), $\langle \Delta r^2(\tau) \rangle = \langle \Delta x^2(\tau) \rangle + \langle \Delta y^2(\tau) \rangle$, where x and y are droplet positions in the horizontal plane, τ is the lag (or waiting) time and $\langle . \rangle$ denotes an average over multiple droplets and time. Except where noted otherwise, we consider only the x and y coordinates because of their lower measurement error without loss of generality, due to the isotropy of our system. The observed MSD has a super-diffusive form, $\langle \Delta r^2(\tau) \rangle \sim \tau^a$, with $a = 1.38 \pm 0.02$, Fig. 2a. The origin of such random motion is not at all obvious. Other properties of the bubble motion (discussed in a later section) are inconsistent with existing models for super-diffusion, such as Lévy walks or chaotic advection [3, 22, 23], or fractional Brownian motion [24]. We do find that smaller droplets move faster than larger droplets (SI Appendix, Fig. 6) consistent with the material acting as a fluctuating mechanical continuum [25].

In an earlier study we showed that super-diffusion in

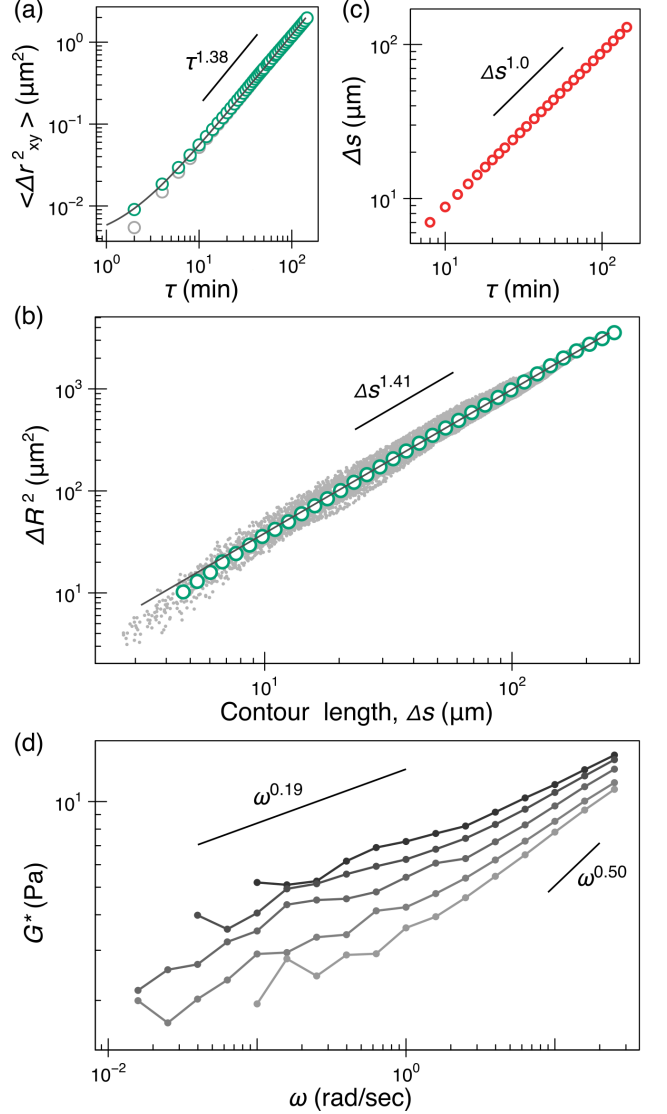


FIG. 2. Analysis of configuration space paths and bulk rheology. (a) Mean-squared displacement (green) of individual droplets. Black line is a fit to a power law plus a constant (measurement error) and grey symbols are the data after subtracting error (see Appendix B). (b) Scatter plot of the squared-separation and contour distance of pairs of configurations (grey) show a fractal scaling after smoothing (green). Black line is a power-law fit for $\Delta s > 20 \mu\text{m}$. (c) The contour and temporal difference between pairs of configurations shows linear scaling, despite the system's intermittent dynamics. (d) Measurements of $G^*(\omega)$ show power-law viscoelasticity at low frequencies, whose exponent agrees mathematically with the observed fractal dimension. Aging times from loading, top to bottom, are 3, 10, 40, 75, 127 minutes.

an SGM model was due to the system following a fractal curve in configuration space [14]. To test that idea with empirical data, we consider a 775-dimensional path constructed from the experimental $x(t)$ and $y(t)$ coordinates of all the droplets. Then, as sketched in Fig. 1a, we consider ‘fragments’ of the path spanning be-

tween all pairs of observed configurations, and compute the ‘size’ ΔR and ‘mass’ Δs of the path fragment. Details of how we reliably compute both the Euclidean distance ΔR and the contour length Δs from noisy experimental data are given in SI Appendix, Fig. 8. Figure 2b shows that these two measures scale with each other obeying a power-law relationship, $\Delta R^2 \sim \Delta s^c$, with $c \approx 1.41 \pm 0.03$. Mathematically, this confirms that the configuration path is a fractal with a corresponding fractal dimension $D_f = 2/c = 1.42 \pm 0.03$, such that mass $\sim (\text{size})^{D_f}$. Simulations show essentially indistinguishable behavior (SI Appendix, Fig. 8).

The relationship between the droplet super-diffusion and the fractal scaling is easy to understand. The configuration path is parameterized by both time t and contour distance s . While intermittent dynamics causes s to increase by varying amounts in a single t interval, the corresponding differences in these variables, Δs and τ , are proportional on average, Fig. 2c. This linear correlation indicates that the high-dimensional mean-squared displacement ΔR^2 will show the same power-law scaling, $\sim \Delta s^c$ and $\sim \tau^c$. Because the individual droplet trajectories are just projections of the configuration space path to lower dimensions, the conventional MSD, $\langle \Delta r^2(\tau) \rangle$, shows the same power-law scaling as well—super-diffusion with the observed exponent satisfying $a \approx c$.

Lastly, the earlier study [14] also predicted a link between the fractal dimension of the configuration path and the material’s power-law viscoelasticity, $G^*(\omega) \sim \omega^\beta$, where ω is the frequency. Specifically, it predicted the relation $\beta = D_f^{-1} - 0.5$. This corresponds to $\beta = 0.20 \pm 0.02$ for the experimental D_f and is consistent with direct measurements of the rheology of age-matched emulsions, Fig. 2d, which show $\beta = 0.19 \pm 0.03$. This confirms that the previously unexplained power-law viscoelasticity of SGMs [26] is also a result of the emergent fractal geometry of the configuration path.

IV. ANOMALOUS DISPLACEMENTS DUE TO LANDSCAPE ANISOTROPY.

A second anomalous feature of soft glassy dynamics can be seen in the probability distribution of random displacements that occur in a given lag time, Fig. 3a, termed the van Hove self-correlation function. For normal random walks, this distribution has a Gaussian shape. The distribution we find here is distinctly non-Gaussian and heavy tailed—large displacements are much more probable than for a Gaussian distribution with the same width. We find that the displacements are well fit for small values by the Lévy alpha-stable distribution, often called the stable distribution (SD), a family of transcendental functions containing the Gaussian function. The SD has power-law tails, with an exponent controlled by the ‘stability parameter’ α , and so contains arbitrarily large (positive and negative) values. In contrast, empirically measured distributions are typ-

ically ‘truncated’ because very large displacements are physically impossible. Indeed, we find empirically that our displacement data are well fit by an exponentially truncated stable distribution (ETSD), see Fig. 3a. The ETSD satisfies $\text{ETSD}(x, \alpha) = \mathcal{A}[\text{SD}(x, \alpha)\exp(-|x|/\lambda)]$, where λ is a truncation length and \mathcal{A} is a normalization constant. Notably, simulation data can also be well fit to the same ETSD form (SI Appendix, Fig. 7). As seen in SI Appendix, Fig. 11, the value of the stability parameter α increases with τ , with an upturn at short τ . Simulations reproduce similar values of α and uptrend, but not the short τ upturn; analysis indicates the upturn is partially due to measurement error and partially due to viscous effects, neither of which is present in the simulation.

As previously with super-diffusion, the physical origin of the non-Gaussian displacements in SGMs is not obvious. The τ -dependence of the shape of the displacement distribution allows us to screen different models. While Lévy walk processes both super-diffuse and can have displacement distributions that resemble truncated stable distributions, their MSD exponent is related to their displacement distribution [23] via $\alpha = 3 - a$. This predicts a τ independent value $\simeq 1.65$ in our case, which is obviously not consistent with the data. Likewise, fractional Brownian motion [24] is super-diffusive, but has a Gaussian van Hove correlation, $\alpha = 2$.

Alternatively, literature models can also predict such heavy-tailed displacement distributions [27, 28]. These argue that a localized droplet rearrangement event creates a predominantly quadrupolar distortion field, which in three dimensions displaces other distant particles in a manner that falls off with distance $\sim r^{-2}$. In this picture, λ would be the typical displacement of a particle undergoing a rearrangement, and the progressively larger numbers of particles at larger distance from the rearrangement would give rise to a power-law tail for values less than λ , with a form $\sim \Delta x^{-2.5}$, corresponding to $\alpha \simeq 1.5$. While more complicated models with spatially extended, non-quadrupolar deformation fields might lead to a slightly different α value, the τ dependence we observe is clearly at odds with the simplest model.

We have found that the heavy-tailed van Hove correlation is closely related to the anisotropy of the configuration space path, as sketched in Fig. 1b. That is, the path taken by the system is not random in directions in configuration space, as might be supposed. We characterize the directions of high-dimensional vectors by converting them to unit length vectors, and then examine the distribution of their vector components, $U_i(t, \tau) = (R_i(t + \tau) - R_i(t))/\Delta R(t, \tau)$. We consider only the y coordinates to calculate U_i since they display the least drift over time. If the original vectors were randomly directed, then this distribution must be very nearly a Gaussian. We analyze the end to end directions of path fragments in this way, for a given value of $\tau = 34$ min, Fig. 3b, which displays minimal perturbations from measurement error. The resulting distribution

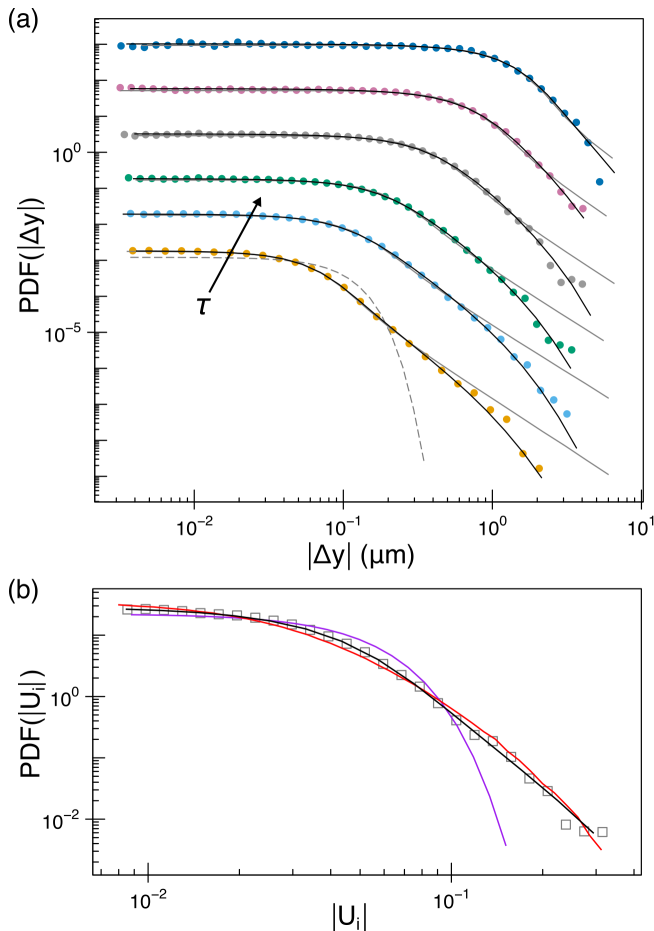


FIG. 3. Probability distributions, or van Hove functions, of droplet displacements are non-Gaussian in both real space and high-dimensional space. (a) The van Hove function of individual droplet displacements for $\tau = 2, 8, 16, 34, 68$, and 140 minutes (bottom to top). Solid black curves represent the best fit ETSD for each τ , grey curves show the best fit SD, and the dashed curve is a best fit Gaussian distribution for $\tau = 2$ minutes. (b) The van Hove function of the components of high-dimensional displacement unit vectors, U_i , for $\tau = 34$ minutes. Black curve is a best fit ETSD to the data. The red curve shows a simple model for the data based on N uncorrelated components with the same ETSD as the data, and the purple curve shows a similar model but with a Gaussian distribution of N components.

is highly non-Gaussian (direct evidence of anisotropy), varies only slightly with τ , and unexpectedly can be fit by an ETSD form very similar to the van Hove distribution, with $\alpha \simeq 1.61$. The directions taken by fractal curves such as the configuration path and branching fractals often display anisotropy (non-random directionality) that is invariant over length-scales. Such direction distributions are another property of a fractal—two fractals may have the same fractal dimension, D_f , and yet appear very different because of differences in their directionality or branching. We hypothesize that the anisotropy of the configuration space path is another emergent fractal

property and presumably related to the geometry of the ‘valleys’ in the underlying energy landscape.

Naïvely, we might suppose that, as with the droplet MSDs, here the ETSD form of the particle van Hove correlation is merely a projection of the high-dimensional unit vector components, and that the two distributions might have the same shape and α values. This turns out not to be the case. A simple model for a high dimensional unit vector would be to generate a set of N *uncorrelated* random components having the same distribution as the van Hove distribution, and then to normalize its length. Analysing the anisotropy of an ensemble of such unit vectors yields a heavy-tailed distribution that closely resembles, but subtly differs from the experimental data. The failure of this construction to yield isotropic unit vectors is a consequence of Lévy statistics (a Gaussian van Hove distribution would yield isotropic unit vectors in this construction). The key difference from the experiment is that this simple model assumes droplet displacements are completely uncorrelated, while the trajectories of pairs of droplets are slightly correlated (either positively or negatively) in a complex, spatially varying manner we will examine in the next section. Still, the near agreement of this simple uncorrelated model with the data suggest that the cooperative motion of droplets is not responsible for the high-dimensional anisotropy and heavy tails in the van Hove, as might have been supposed, but merely perturbs both distributions.

V. AVALANCHES DUE TO FRACTAL CLUSTERING OF MINIMA.

The motion of droplets in an SGM appears intermittent and highly cooperative, with many particles moving abruptly at the same time. A simple way to quantify such cooperativity is to count how many droplets move more than a threshold amount in a time interval. A threshold of λ should isolate those droplets undergoing the largest rearrangements. We choose a lower threshold $\lambda/2$ for improved statistics. Figure 4a shows the number of droplets that move more than that threshold, $N_{\lambda/2}(t)$, in the time interval between consecutive image scans, as a function of time. This function shows large peaks at times when many droplets make large motions. Moreover, a plot of the probability distribution $P(N_{\lambda/2})$ in Figure 4a(inset) shows a heavy-tailed form, varying as $P(N_{\lambda/2}) \sim (N_{\lambda/2})^{-1.4}$. If every particle moved independently of the others, this distribution would have a different (binomial) distribution. Based on the idea that cooperativity consists of some rearrangements triggering others, such large, power-law distributed rearrangement events are commonly called avalanches, analogous to those in snow or sand.

A common method to visualize the spatial arrangement of such rearrangements is to prepare a movie that renders only the most mobile droplets, for example using a threshold such that 5% of droplets appear on a

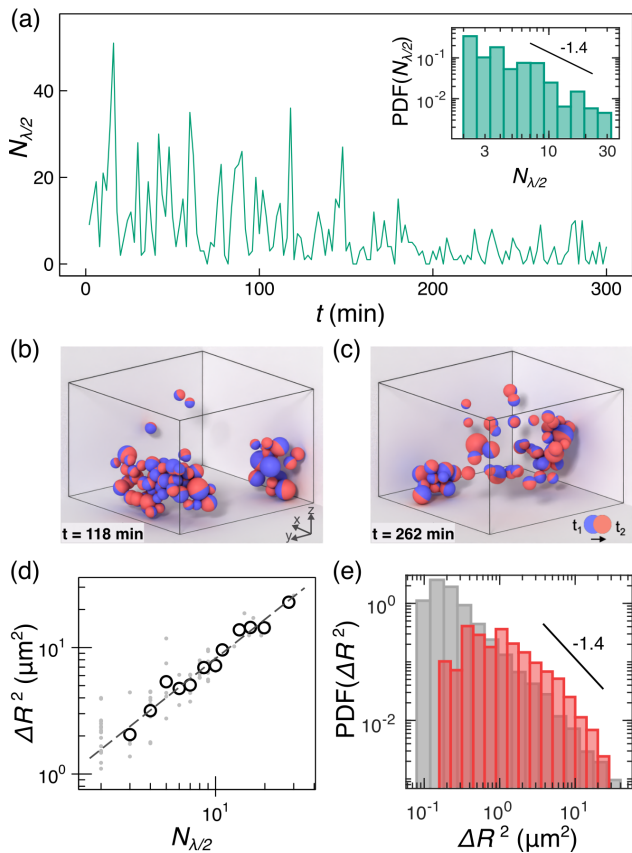


FIG. 4. (a) Number of droplets moving by $\Delta x, \Delta y > \lambda/2$ at each time point. Inset shows the probability distribution of these values, following a power law with slope of -1.4 ± 0.1 . (b,c) Renders of droplets that move in the top 5% of all displacements reveal localized clusters during large avalanche events. (d) ΔR^2 for $\tau = 2\text{min}$, normalized by the mean radius at each t and removing measurement error, scales linearly with $N_{\lambda/2}$. Dashed line is a power law fit with slope of 1.0. (e) The probability distribution of ΔR^2 also follows a power law with slope of -1.4 ± 0.1 , matching that of $N_{\lambda/2}$ and the simulation data (grey distribution).

time-averaged basis, see SI Appendix, Movie S2. Corresponding images for two typical large avalanches are shown in Figs. 4b,c. To indicate the direction of the droplet motions, the final location of each droplet is rendered in red, the starting location in blue. Because the displacements are small, most droplets render as slightly displaced red and blue hemispheres. Rendering of simulation data yields similar results (SI Appendix, Fig. 9). Closer examination reveals the avalanches have a complex spatial structure, forming extended, nearly dense clusters of neighboring droplets. Such clustering is qualitatively similar to the dynamical heterogeneity seen in the cooperative Brownian motion of dense colloidal fluids [29]. Further analysis reveals that the number of droplets participating in each cluster follows a power-law distribution, and that the clusters themselves are fractal [29] with dimension $D_f \simeq 2.50$, see SI Appendix, Fig. 9.

Again returning to the high-dimensional analysis, we seek to understand what features of the energy landscape give rise to avalanche-like cooperative dynamics. Notably, we find that avalanches correspond to large high-dimensional Euclidean displacements, ΔR , between two consecutive points in configuration space. In fact, the two measures of avalanche size are proportional: $\Delta R^2 \propto N_{\lambda/2}$, as shown in Fig. 4d. Since the $N_{\lambda/2}$ values are power-law distributed, this correlation implies that ΔR^2 should be as well; indeed, we find $P(\Delta R^2) \sim (\Delta R^2)^{-1.4}$, shown in Fig. 4e.

Recall that the emulsion relaxes rapidly from one stable energy minimum (where the forces between droplets are in balance) to another, spending most of its time arrested at a minimum. As a result, experimental observations should typically correspond to energy minima. Thus, the measured $P(\Delta R^2)$ between consecutive images may effectively be reporting the distribution of distances between minima of the energy landscape itself, as sketched in Fig. 1c. Of course, multiple avalanches may occur between (or during) microscope scans of the sample, so the ΔR^2 between measurements may ‘skip’ some closely spaced minima. Matched simulations confirm this idea, and shows that the limited temporal sampling rate of the experiments does not significantly alter the power-law exponent of $P(\Delta R^2)$. Indeed, measurements of ΔR^2 between consecutive energy minima in the simulation yield very similar results to the experimental $P(\Delta R^2)$, at least for the largest ΔR^2 , see Fig. 4e.

The observed power-law distribution of distances between minima ΔR^2 is unusual. Were the energy minima distributed randomly along the path, the corresponding distribution would have an exponential form. Rather than being random, the power-law distribution of ΔR^2 indicates that the energy minima along the path are clustered, and that these clusters have a fractal structure. In an earlier study, we found that minima are preferentially located in regions of configuration space where the energy landscape is almost flat on longer lengthscales [14]. Thus, the observed fractal distribution of energy minima, that is responsible for the heavy-tailed distribution of avalanche sizes, is likely a manifestation of the underlying fractal structure of the energy landscape itself, a feature observed theoretically in disordered systems in high dimensions [30–35].

VI. LANDSCAPE DYNAMICS OF STOCK PRICES.

The random fluctuations of stock prices have previously been compared to several different random processes, many of them drawn from statistical physics. The Black-Scholes equation [9, 10] is a modified Langevin equation similar to that describing Brownian motion. Other authors have compared price motions to the deterministic chaos of turbulent fluid flow [11, 12] or Lévy processes [13] with varying degrees of success. Still oth-

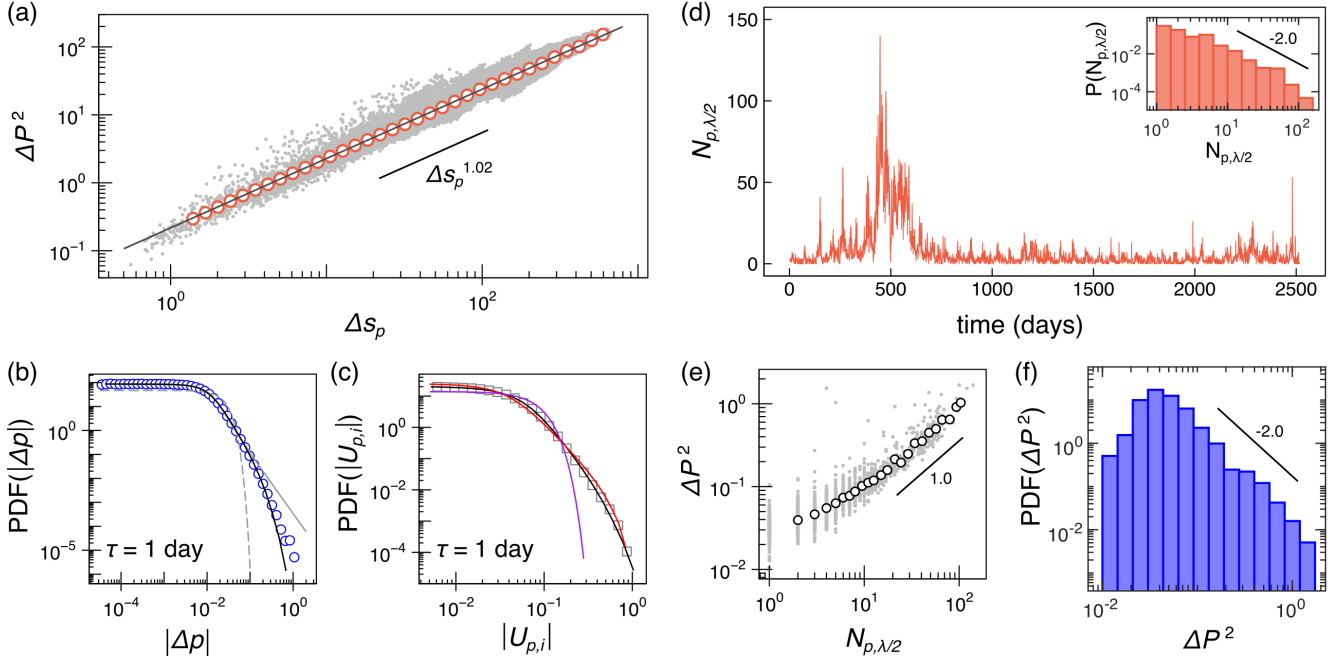


FIG. 5. (a) Scatter plot of the high-dimensional price returns and contour distance between pairs of configurations. Line is a power-law fit with slope of 1.02 to the data after smoothing (orange circles). (b) van Hove function of individual stock price returns for $\tau = 13$ days. Curves show the best fit ETSD (solid black), SD (solid grey) and Gaussian (dashed grey). (c) van Hove function of the components of high-dimensional displacement unit vectors for $\tau = 13$ days. Curves show the best fit ETSD (black), a model based on ETSD uncorrelated components (red), and a similar model based on Gaussian distributed uncorrelated components (purple). (d) Number of stocks with $\Delta p > \lambda_p/2$ each day. Inset shows the probability distribution of $N_{\lambda_p/2}$, which follows a power law with slope of -1.6 ± 0.1 . (e) Linear scaling of $N_{\lambda_p/2}$ and ΔP^2 at $\tau = 1$ day. Dashed line is a fit with slope of 0.97 to the data after smoothing (black circles). (f) Probability distribution of ΔP^2 at $\tau = 1$ day also follows a power law with slope of -1.6 ± 0.1 .

ers have compared the price motion to the avalanches in self-organized criticality (SOC) models [36, 37] or recently, the many-body fluctuations of soft matter systems [38]. Typically, the price motions resemble the physical processes in some ways, and not in others [12, 39], and it is often difficult to relate these findings to traditional concepts in economics theory.

Here we argue that the price motions of the component stocks of the SP500 index closely resemble the above described motion of droplets in SGMs, including similar features in a high-dimensional ‘price configuration space’. Stock price motions have previously been shown to be heavy-tailed [40–43], and to be prone to avalanche-like cooperative moves [36, 38]. Classically, the fluctuating price of a single stock is considered to be the result of a simple equilibrium between supply and demand for stocks of that one company. Our findings suggest instead that the price making process is high-dimensional, consisting of many different companies competing for the same funds, with trading seeking to maximize total market value, perhaps akin to droplets exchanging elastic energy to minimize total energy. We can probe the geometry of such a hypothetical high-dimensional ‘value landscape’ by examining the price motions in high-dimensional space and find, remarkably, that the value

landscape has an emergent fractal geometry similar to the energy landscape of SGMs.

We considered the daily closing price data for the component companies of the Standard and Poor’s 500 index (SP500) over the decade spanning from January 2007 to December 2016. We remove those companies that were dropped or added to the index during this interval, as well as those with infrequent trading, leaving an ensemble of 304 companies. These price trajectories were corrected for splits, converted to logarithmic prices, with returns being the difference in log price during a time interval, typically one trading day. Unlike the SGM case, we find that the return trajectories for different stocks are highly correlated with one another; which has been attributed to the correlated demand created by trading of SP500 index funds (see SI Appendix, Fig. 10 for correlation analysis). These correlations are termed index cohesive and adhesive effects, respectively, with the ‘market mode’ effect being responsible for most of the correlation between component stock returns [44, 45]. Since we are not interested here in the dynamics of the index, which has been studied by others [43, 46], we remove the market mode from the component stock prices by linear regression (see SI Appendix). This results in an ensemble of ‘corrected’ log prices that have about half the fluctuation variance or

‘power’ compared to the original prices and are uncorrelated with the index price (by construction). Consistent with our hypothesis, the motion of these prices is both positively and negatively correlated with one another in a manner that closely resembles that seen in the SGM droplet trajectories. This log price ensemble is then linearly detrended to remove its center of mass motion (due to secular growth of the market) and the resulting 304 time-dependent log price trajectories, $p_i(t)$, are then analyzed as if they were droplet coordinates.

The geometry of the SP500 index components’ path in the 304-dimensional ‘price space’ was analysed by comparing the high-dimensional Euclidean distance, $\Delta P(t, \tau) = ||\vec{P}(t + \tau) - \vec{P}(t)||$, to the path length Δs_p , and found to be a high-dimensional fractal, as in the SGM case, over more than a decade of price distance with $D_f = 1.96 \pm 0.03$, see Fig. 5a. This value corresponds to that of a random walk fractal $D_f = 2$ in high-dimensional space. The corresponding ensemble averaged MSD of the log prices was diffusive, $\Delta p^2(\tau) \propto \tau$, as commonly reported in the literature [47]. This fractal dimension is sensible—a different value would imply long-time correlations in the price motions, which would be subject to arbitrage [48].

Second, the self van Hove correlation of the log price motion, or the returns, $P(\Delta p(\tau))$, closely resembled the SGM case. The distribution was well fit by an ETSD form, Fig. 5b, with a stability parameter $\alpha_p = 1.31$ for $\tau = 1$ day. Interestingly, the distributions for both positive and negative returns are very similar, which is not the case for the index motion. The ETSD form resembles other reported empirical forms such as a stable distribution with a different truncation [13] and the ‘inverse cubic law’ [49–51]. The few outliers from the fit in the tail correspond to $> 30\%$ daily price motions, unusually volatile stocks, mostly during the height of the financial crisis and correspond to fewer than 0.005% of daily trades. A directionality analysis for the price space path, as in Fig. 1b, finds anisotropy resembling the SGM case. The direction components again yield an ETSD distribution, see Fig. 5c, with $\alpha \approx 1.42$, indicating that price motions are highly anisotropic in price space. A simple model consisting of uncorrelated ETSD price motions nearly predicts the observed anisotropy, with small deviations that resemble the corresponding SGM case, presumably due to the perturbative effects of cooperative price motion.

Lastly, the motion of stocks was found to be highly cooperative. Since positive and negative motions are considered together, this reflects fluctuations in the volatility of the component prices rather than ‘crashes’ per se. The number of price motions exceeding $\pm \lambda_p/2$, $N_{\lambda_p/2}$ shows large fluctuations, Fig. 5d, where λ_p is the truncation parameter from fitting the self van Hove distribution. The probability distribution $P(N_{\lambda_p/2})$ has a power-law form, similar to the avalanche behavior in SGMs, with a steeper exponent, Fig. 5d(inset). The distances in high-dimensional price space between daily closes, ΔP , was found to be correlated with the number of stocks mak-

ing large excursions, Fig. 5e, asymptoting to the same relationship seen in SGMs, $\Delta P^2 \propto N_{p, \lambda/2}$. This causes its distribution $P(\Delta P^2)$ to also have a power-law form, see Fig. 5f, with an exponent slightly different from the SGM case. As with SGMs, this power-law distribution indicates that points of transient price equilibrium have a fractal distribution in price space.

Our results confirm our hypothesis regarding stocks executing a value maximization process on a fractal value landscape. The high-dimensional price space trajectory could be supposed to spend much of its time at stable value maxima, at which the prices of different companies are transiently in competitive balance. Those equilibria are however being continuously destabilized by slow changes of economic and competitive factors (akin to ripening in the SGM case) leading to abrupt transitions from the newly unstable equilibrium to a nearby stable one (akin to an avalanche). In between price equilibria, the market follows fractal valleys in the landscape to manifest as intermittent random price motions.

One difference between stock returns and droplet motion is that the destabilization process is unsteady in the stock case. This explains the bursts of intermittency in Fig. 5d, which persist over different time scales. This phenomenon is termed *volatility clustering* [48, 52], and is presumed to be driven by external pressures and shocks to the economy and competitive environment. Of course, no such external perturbations were present in our quiescent emulsion. Multiple models take volatility clustering into account, such as the GARCH model [53], describing the process as stationary with a time-varying conditional variance.

VII. DISCUSSION AND OUTLOOK

The recurrence of the random fractal dynamics we report here (and associated SGM phenomena) in seemingly unrelated systems including foams and emulsions, the stock market, and perhaps cytoskeletal networks [8] and neural networks [54, 55] suggests they share in common a deep mathematical origin. By analogy, single degrees of freedom subjected to noise (such as Brownian motion) almost universally converge to a random walk having diffusive dynamics and a Gaussian van Hove distribution, as explained by the Central Limit Theorem. In systems with fractal dynamics, all that is required is a fractal high-dimensional surface describing the constraints among many degrees of freedom, relaxation kinetics that are much faster than the slow changes of the landscape (which destabilize extrema) [14], and negligible noise. While the kinetic and noise factors can easily be met by many systems, the similarity of the emergent properties of the fractal landscapes of such different systems has no obvious explanation.

The systems with fractal dynamics have in common strong interactions mediated by a dynamically changing, disordered network of connections. In the emulsion,

the network of contacting droplets evolves dynamically due to ripening. In the cytoskeleton, the network of tensed polymer filaments is continuously being remodeled by enzymatic processes. In the economy, the network describing the degree of competition between different companies slowly evolves. We conjecture that the emergent fractal (or self-similar) properties of the landscape may be related to the mathematics of such random and sometimes self-similar networks. In the sphere packing problem and in a simple neural network model termed the Perceptron, the energy and loss landscapes were found to closely correspond [56], and to resemble a high-dimensional polyhedron or polytope. Thus, our findings may be a feature of the generic self-similarity [31, 57] of such random polytopes or their associated networks.

We expect the exploration of high-dimensional landscapes from empirical data will prove useful in a variety of systems with similar dynamics. Future application of our analyses to stock price motions (or high-dimensional commercial data in general) could enable superior models for risk and derivative pricing, or market analysis. High resolution multi-particle tracking data in cells [58, 59] may enable the characterization of the cytoskeleton's energy landscape, enabling a deeper understanding of cytoskeletal physics. Lastly, practical applications of AI rely on deep learning, where computationally costly learning processes are accelerated by 'shortcut' connections [60] in the network, which alter the structure of the high-dimensional 'loss' landscape. Our analysis may lead to a clearer understanding of deep learning dynamics [55], and more efficient learning algorithms.

ACKNOWLEDGMENTS

We are grateful for useful conversations with Doug Durian, François Lavergne, Andrea Liu, Christopher Porter, Yu Shi, Talid Sinno, Veronique Trappe and Eric Weeks. We are also grateful to Dr. Bomyi Lim for confocal microscopy and Dr. Paulo Arratia for rheometry. This work was supported by NSF-DMR 0706388, 1609525, 1720530 and 1915193 and the David and Lucile Packard Fellowship with computational resources provided by XSEDE through TG-DMR150034.

Appendix A: Materials and Methods

Sample preparation: The O/W emulsion was prepared by slow, dropwise addition of the dispersed phase (80% v/v) to the continuous phase with constant homogenization (IKA T18) at 21,500 rpm. The continuous phase contained 3% (w/w) Synperonic PE P105 (Sigma-Aldrich) surfactant dissolved in a mixture of 95% (w/w) formamide, 5% (w/w) water. For confocal imaging fluorescein sodium salt was dissolved in the water component at 2.7 mM concentration, prior to mixing and emulsifi-

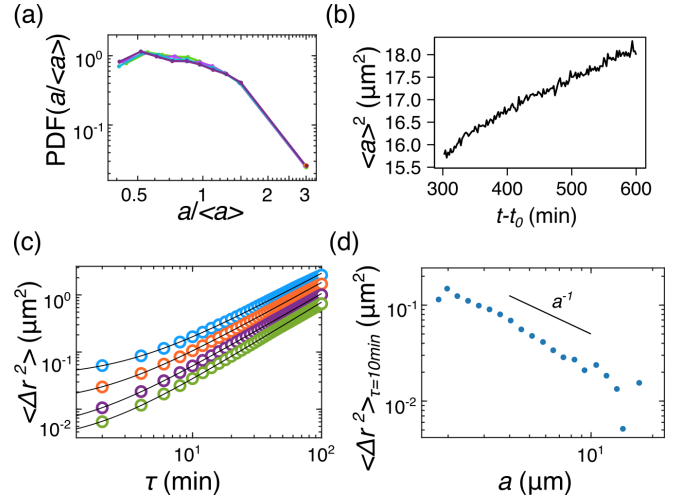


FIG. 6. Experimental system agrees with expected dynamical scaling behavior and polydispersity effects. (a) Droplet size distribution evolution throughout the dynamical scaling period, normalized by the average droplet size, where $t - t_0$ represents time from the beginning of data collection and $t_0 = 7$ hrs is the time from emulsification. (b) Time evolution of the squared average droplet radius shows expected linear relationship. (c) Mean squared displacement of droplet ensembles grouped by radii: $[1.60\text{-}2.65] \mu\text{m}$ (blue), $(2.65\text{-}3.79) \mu\text{m}$ (orange), $(3.79\text{-}5.33) \mu\text{m}$ (purple), $(5.33\text{-}18.21) \mu\text{m}$ (green). Black curves show fits to a power law plus a constant $y = ax^b + c$, where $c = 2\sigma^2$ and σ represents measurement error. The displacements of smaller droplets contain larger error, as expected, due to image resolution limitations. (d) Mean squared displacement at $\tau = 10$ min as a function of droplet radius follows the expected $a - 1$ behavior.

cation. The dispersed phase contained a mixture of 94% (w/w) 1-bromohexane and 6% (w/w) octane. Following emulsification, the sample was centrifuged for 10 minutes at 700 rpm for removal of air bubbles, and was aged in a closed microscopy chamber at room temperature. This chamber consisting of stacked #1.5 coverslips used as spacers, topped by a #0 coverslip and sealed with high viscosity UV glue (Norland 68T). The dense emulsion was then imaged using a Zeiss LSM 800 confocal microscope with an oil immersion objective;

Figure 6 confirms that the system has reached a dynamical scaling state, where the squared droplet size increases linearly with time and the shape of the size distribution does not change significantly (Figs. 6a,b). As expected for droplets in a mechanical continuum, larger droplets diffuse more slowly (Figs. 6c,d), showing the same scaling as the Stokes-Einstein relation despite being driven by active stress fluctuations.

Rheology: Measurements were performed using a strain-controlled rheometer (DHR-3 TA Instruments) with a parallel plate geometry (40 mm plate diameter). All measurements were done in the linear viscoelastic regime (strain $\epsilon = 1\%$), which was verified by an amplitude sweep at $\omega = 1$ rad/sec. Complex shear

modulus values were obtained from frequency sweeps at $T = 25 \pm 1^\circ\text{C}$ and frequencies from $\omega = 0.016$ to 30 rad/sec. The gap size ranged from 90 - 150 μm and the same sample was measured multiple times to observe the effects of emulsion aging. Frequency scans in both directions (from low to high ω and vice versa) showed similar results and were averaged together. Measurements were started 7 hours after emulsion preparation to reach dynamical scaling and to correspond to the confocal imaging data.

Stock price motion: Price motions from the SP500 stock index and its components were used for this analysis, only utilizing components that were part of the index throughout the entire time span being considered. Daily closing price data (years 2007-2017), corrected for splits, was retrieved from the Wharton Research Data Services (WRDS) platform at the University of Pennsylvania.

To linearize exponential trends and remove scale differences between different stock prices, the raw price trajectories were log-transformed into log price trajectories. Weekends and overnight gaps in the data (closed market hours) were assumed to have negligible contributions to a stock's trajectory. For example, a price return from Friday to Monday was still considered $\Delta t = 1$ day. To remove index cohesive and adhesive effects, we performed a simple subtraction of the index from the daily returns, similar to that discussed by Borghesi et. al [44]. We assume that the log-return of each component i at a given time is composed of 2 terms, $\Delta p_{i,corr}(t) = \Delta p_i + \beta_i I(t)$, where $\Delta p_{i,corr}$ is the correlated return, β_i is the Pearson correlation coefficient, $I(t)$ is the index return, and Δp_i is the uncorrelated return that we will use for comparison to the SGM data.

The de-correlated returns, Δp_i , were then detrended by subtracting the average linear motion of the entire ensemble over the duration of the sample (corresponding to the mean exponential growth with a CAGR of 5.5%). All variables shown in Fig. 5 were calculated using these log-transformed returns in place of droplet coordinates.

Emulsion Simulation: We simulate our dense emulsion using a modified 3-D bubble model, extending the one used in our previous study [14], based on a system of polydisperse soft-spheres at a volume fraction $\phi = 0.75$, with pairwise interaction energy:

$$V(\mathbf{d}_{ij}) = \begin{cases} \frac{\epsilon}{2} \left(1 - \frac{\|\mathbf{d}_{ij}\|}{r_i + r_j}\right)^2, & \text{if } \|\mathbf{d}_{ij}\| < r_i + r_j \\ 0, & \text{otherwise,} \end{cases} \quad (\text{A1})$$

\mathbf{d}_{ij} being the distance between two bubbles (soft-spheres) of radii r_i and r_j . The bubbles exchange mass due to differences in notional Laplace pressure according to:

$$Q_i = -\alpha_1 \sum_j^{\text{neighbors}} \left(\frac{1}{r_i} - \frac{1}{r_j}\right) A_{\text{overlap}} - \alpha_2 \left(\frac{1}{r_i} - \frac{1}{\langle r \rangle}\right) r_i \quad (\text{A2})$$

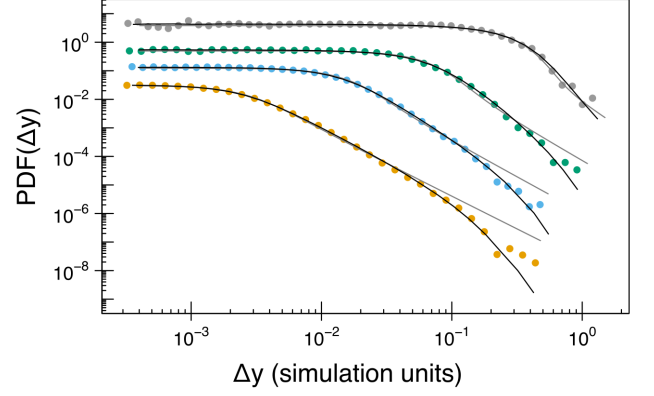


FIG. 7. van Hove function of simulation droplet displacements for $\tau = 1, 5, 24$, and 140 simulation time units (bottom to top). Solid black curves represent the best fit ETSD and grey curves show the best fit SD.

The evolution of the system is considered in the quasi-static limit - where the energetic relaxation time is much smaller than the ripening time scale. This leads us to relax the system to a minimum between consecutive ripening moves. The parameters for the simulation are similar to Ref. [14]. The system is initialized using a Gaussian distribution of bubble radii and its properties are considered once the system reaches a dynamical scaling state. To efficiently simulate larger system sizes, we implement a custom neighbor list algorithm suitable for evolving polydisperse systems. Our modified cell list algorithm associates the droplets with cells and associates interacting neighbors using a cell list. Further, we use a buffer length search for potential neighbors and update our neighbor list when the radii changes and displacements exceed this buffer length, cumulatively enabling $\mathcal{O}(N \log N)$ operations for N droplets. The droplets eventually reach a steady-state radii distribution resembling a Weibull distribution, $P(r) = (k/\Lambda)(r/\Lambda)^{k-1} \exp(-(r/\Lambda)^k)$, where $k \approx 1.66$ and Λ is a scale parameter.

Figure 7 shows the distribution of droplet displacements in simulations, for multiple values of τ . These are well fit by an ETSD, and the α values from the fits follow a time-varying trend similar to the experimental data (SI Appendix, Fig. 11).

Appendix B: Measurement Error

The experimental measurement error can be quantified by fitting the mean-squared displacement of individual droplets to a power law plus a constant, $MSD_{xy} = A\tau^B + C$, where $C = 4\sigma^2$. The fit is shown in Fig. 1a, where $4\sigma^2 = 0.0036$ μm^2 and $\sigma = 0.03$ μm . This presumably perturbs high-dimensional displacement calculations, especially for low values of τ . To show how random error affects our data, we added a Gaussian-

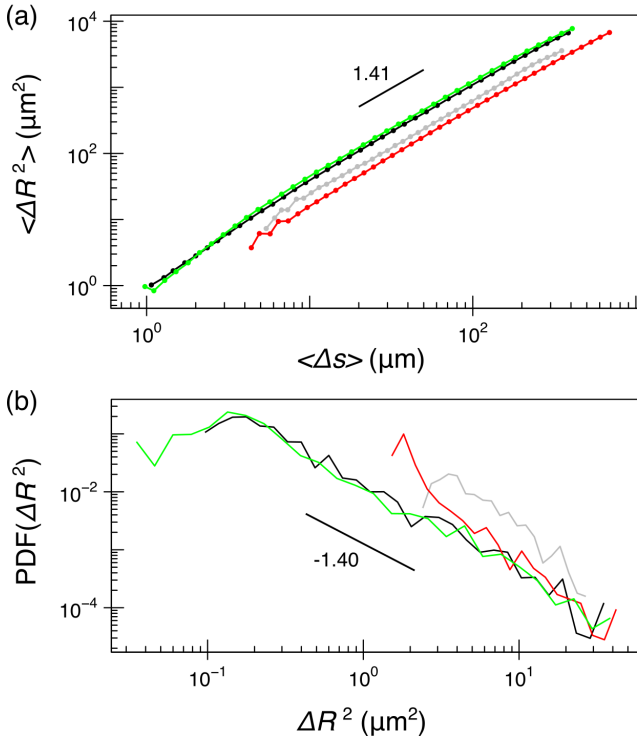


FIG. 8. Removing Gaussian noise effects from high-dimensional displacements. (a) ΔR^2 and Δs between pairs of simulation configurations (black), simulation after adding Gaussian noise (red), and simulation with Gaussian noise after using the noise removal method described in the text (green). Experiment results before removing measurement error are shown in grey. (b) Probability distribution of ΔR^2 for $\tau = 1$ simulation time step and $\tau = 1$ min in the experiment. Color scheme is the same as (a).

distributed noise signal with zero mean and $\sigma = 0.03 \mu\text{m}$ to the noise-free simulation data (re-scaled for comparison to the experiment). As shown in Fig. 8a, Gaussian error significantly alters the original simulation results by omitting the smallest displacements. To remove this effect, we modified the calculation of all high-dimensional displacements to exclude all dimensions that are below a certain threshold. We found that a threshold of 4σ was necessary for the noisy data to revert back to its original curve. Similar results are shown in Fig. 8b for the distribution of ΔR^2 at $\tau = 1$ simulation time step, where noise completely changes the shape and slope of the distribution. This modified calculation was therefore applied to the experimental ΔR^2 and Δs values throughout our analyses in order to reduce systematic errors due to noise in the results.

Appendix C: Avalanche Clusters

The droplets with the largest displacements between consecutive confocal images ($\tau = 2$ min) were determined by using a time-dependent threshold, constructed so that

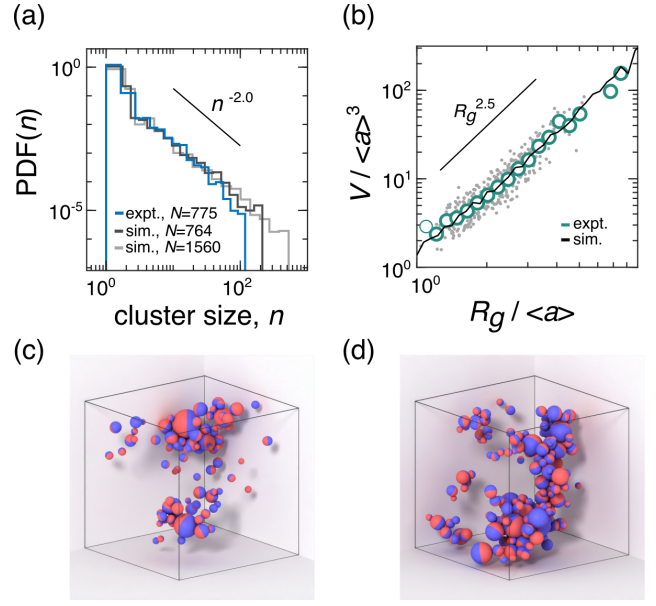


FIG. 9. Cluster analysis for droplets with the largest displacements. (a) Distribution of the number of droplets, n , in each cluster shows power law scaling for both experiment and simulation. (b) The volume of individual clusters, V , shows a power law dependence on their radius of gyration, R_g , confirming their fractal shape and matching the averaged simulation results (line). Green circles are averages of the grey data points. (c,d) Simulation data renders of the particles moving in the top 5% of all particles at 2 different time points, calculated with the same threshold method described in the text.

5% of droplets were above threshold on a time averaged basis. These particles were formed into clusters using an adjacency matrix that specifies which droplets are contacting neighbours. Droplets were considered to be in contact if their center-to-center separation was less than 1.1 times the sum of their radii, to allow for measurement error and droplet distortion. Our findings were not sensitive to this factor. The resulting clusters from the

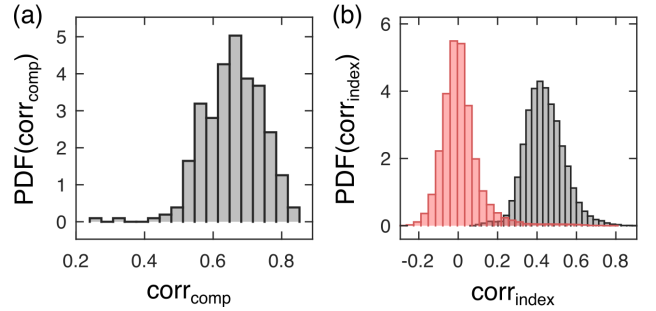


FIG. 10. Distributions of Pearson correlation coefficients for the stock trajectories. (a) Pearson coefficient between each stock and the index trajectory. (b) Pearson coefficient between all possible pairs of stocks before (grey) and after (red) subtracting the index mode.

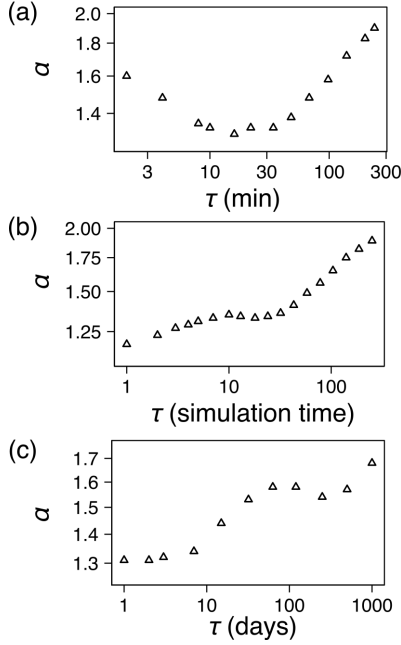


FIG. 11. ETSD stability parameter, α , for the lag-time dependent van Hove displacement distributions from the emulsion experiment (a), emulsion simulation (b), and component stock log price returns (c).

experiment show fractal scaling (Figs. 9a,b) and are similar to those observed in the simulations (Figs. 9c,d).

Appendix D: Stock Correlations

The component return trajectories of a market index are known to have a significant positive average correlation with their index return trajectory [44], presum-

ably due to cash flows produced by trading the index rather than the component company's stock. The distribution of stock-Index correlation coefficients in our data (Fig. 10a) confirms this behavior with an average of $\langle \text{corr}_{\text{index}} \rangle = 0.66$. Correspondingly, a component's return trajectory is expected to have a positive average correlation with the rest of the index components. The distribution of correlation coefficients for all pairs of stocks, shown in Fig. 10b, also confirms this idea with an average of $\langle \text{corr}_{\text{comp}} \rangle = 0.44$. After subtracting the index mode from our data (see Appendix A for methods), the correlations are reduced to an average that is close to zero, $\langle \text{corr}_{\text{comp}} \rangle = 0.01$. Since the droplets in the emulsion system are not correlated with each other via their correlations to an external factor (such as their center of mass), we hypothesize that our droplet model provides a description only of the component price motions with the index subtracted, and not the dynamics of the index itself.

Appendix E: ETSD Stability Parameter

We have found that an exponentially truncated stable distribution (ETSD) provides a useful fitting form for the van Hove distribution in systems with fractal landscape dynamics, as shown in Figures 3, 5 and 7. The stability parameter α from those fits provides a measure of how heavy-tailed the distribution is, related to the exponent of the power-law tail in the untruncated SD. These α values show a non-trivial τ dependence, shown in Figure 11. All three appear to be trending to a Gaussian value $\alpha = 2$ at long times. The disagreement at short times between the emulsion simulation and experiment can be rectified by adding viscous damping to the simulation, and will be discussed in a future publication.

-
- [1] J. Renn, Einstein's invention of Brownian motion, *Annalen der Physik* **14**, 23 (2005).
 - [2] H. G. Schuster and W. Just, *Deterministic chaos: an introduction* (John Wiley & Sons, 2006).
 - [3] V. Zaburdaev, S. Denisov, and J. Klafter, Lévy walks, *Reviews of Modern Physics* **87**, 483 (2015).
 - [4] A. Gopal and D. J. Durian, Nonlinear bubble dynamics in a slowly driven foam, *Physical Review Letters* **75**, 2610 (1995).
 - [5] P. Hébraud and F. Lequeux, Mode-coupling theory for the pasty rheology of soft glassy materials, *Physical Review Letters* **81**, 2934 (1998).
 - [6] P. Sollich, F. Lequeux, P. Hébraud, and M. E. Cates, Rheology of soft glassy materials, *Physical Review Letters* **78**, 2020 (1997).
 - [7] B. Fabry, G. N. Maksym, J. P. Butler, M. Glogauer, D. Navajas, and J. J. Fredberg, Scaling the microrheology of living cells, *Physical review letters* **87**, 148102 (2001).
 - [8] B. D. Hoffman and J. C. Crocker, Cell mechanics: dissecting the physical responses of cells to force, *Annual Review of Biomedical Engineering* **11**, 259 (2009).
 - [9] M. Scholes and F. Black, The pricing of options and corporate liabilities, *Journal of Political Economy* **81**, 637 (1973).
 - [10] H. Föllmer, Stock price fluctuation as a diffusion in a random environment, *Philosophical Transactions of the Royal Society of London. Series A: Physical and Engineering Sciences* **347**, 471 (1994).
 - [11] S. Ghashghaie, W. Breymann, J. Peinke, P. Talkner, and Y. Dodge, Turbulent cascades in foreign exchange markets, *Nature* **381**, 767 (1996).
 - [12] R. N. Mantegna and H. E. Stanley, Turbulence and financial markets, *Nature* **383**, 587 (1996).
 - [13] R. Cont, M. Potters, and J.-P. Bouchaud, Scaling in stock market data: stable laws and beyond, in *Scale invariance and beyond* (Springer, 1997) pp. 75–85.

- [14] H. J. Hwang, R. A. Riggleman, and J. C. Crocker, Understanding soft glassy materials using an energy landscape approach, *Nature Materials* **15**, 1031 (2016).
- [15] J. Clara-Rahola, T. Brzinski, D. Semwogerere, K. Feitosa, J. Crocker, J. Sato, V. Breedveld, and E. R. Weeks, Affine and nonaffine motions in sheared polydisperse emulsions, *Physical Review E* **91**, 010301 (2015).
- [16] R. Penfold, A. D. Watson, A. R. Mackie, and D. J. Hibberd, Quantitative imaging of aggregated emulsions, *Langmuir* **22**, 2005 (2006).
- [17] P. Stevenson, Inter-bubble gas diffusion in liquid foam, *Current Opinion in Colloid & Interface Science* **15**, 374 (2010).
- [18] K. Feitosa, O. L. Halt, R. D. Kamien, and D. J. Durian, Bubble kinetics in a steady-state column of aqueous foam, *EPL (Europhysics Letters)* **76**, 683 (2006).
- [19] D. J. Durian, Foam mechanics at the bubble scale, *Physical Review Letters* **75**, 4780 (1995).
- [20] S. Tewari, D. Schiemann, D. J. Durian, C. M. Knobler, S. A. Langer, and A. J. Liu, Statistics of shear-induced rearrangements in a two-dimensional model foam, *Physical Review E* **60**, 4385 (1999).
- [21] I. K. Ono, S. Tewari, S. A. Langer, and A. J. Liu, Velocity fluctuations in a steadily sheared model foam, *Physical Review E* **67**, 061503 (2003).
- [22] T. Solomon, E. R. Weeks, and H. L. Swinney, Observation of anomalous diffusion and lévy flights in a two-dimensional rotating flow, *Physical Review Letters* **71**, 3975 (1993).
- [23] E. R. Weeks and H. L. Swinney, Anomalous diffusion resulting from strongly asymmetric random walks, *Physical Review E* **57**, 4915 (1998).
- [24] B. B. Mandelbrot and J. W. Van Ness, Fractional Brownian motions, fractional noises and applications, *SIAM review* **10**, 422 (1968).
- [25] A. W. Lau, B. D. Hoffman, A. Davies, J. C. Crocker, and T. C. Lubensky, Microrheology, stress fluctuations, and active behavior of living cells, *Physical Review Letters* **91**, 198101 (2003).
- [26] F. A. Lavergne, P. Sollich, and V. Trappe, Delayed elastic contributions to the viscoelastic response of foams, *The Journal of Chemical Physics* **156**, 154901 (2022).
- [27] L. Cipelletti, L. Ramos, S. Manley, E. Pitard, D. A. Weitz, E. E. Pashkovski, and M. Johansson, Universal non-diffusive slow dynamics in aging soft matter, *Faraday Discussions* **123**, 237 (2003).
- [28] D. W. Swartz and B. A. Camley, Active gels, heavy tails, and the cytoskeleton, *Soft Matter* **17**, 9876 (2021).
- [29] E. R. Weeks, J. C. Crocker, A. C. Levitt, A. Schofield, and D. A. Weitz, Three-dimensional direct imaging of structural relaxation near the colloidal glass transition, *Science* **287**, 627 (2000).
- [30] C. P. Massen and J. P. Doye, Power-law distributions for the areas of the basins of attraction on a potential energy landscape, *Physical Review E* **75**, 037101 (2007).
- [31] P. Charbonneau, J. Kurchan, G. Parisi, P. Urbani, and F. Zamponi, Fractal free energy landscapes in structural glasses, *Nature Communications* **5**, 1 (2014).
- [32] H. Yoshino and F. Zamponi, Shear modulus of glasses: Results from the full replica-symmetry-breaking solution, *Physical Review E* **90**, 022302 (2014).
- [33] C. Rainone, P. Urbani, H. Yoshino, and F. Zamponi, Following the evolution of hard sphere glasses in infinite dimensions under external perturbations: Compression and shear strain, *Physical Review Letters* **114**, 015701 (2015).
- [34] G. Biroli and P. Urbani, Breakdown of elasticity in amorphous solids, *Nature Physics* **12**, 1130 (2016).
- [35] P. Charbonneau, J. Kurchan, G. Parisi, P. Urbani, and F. Zamponi, Glass and jamming transitions: From exact results to finite-dimensional descriptions, *Annual Review of Condensed Matter Physics* **8**, 265 (2017).
- [36] M. Bartolozzi, D. B. Leinweber, and A. W. Thomas, Scale-free avalanche dynamics in the stock market, *Physica A: Statistical Mechanics and its Applications* **370**, 132 (2006).
- [37] A. E. Biondo, A. Pluchino, A. Rapisarda, and D. Helbing, Reducing financial avalanches by random investments, *Physical Review E* **88**, 062814 (2013).
- [38] A. M. Puertas, M. A. Sánchez-Granero, J. Clara-Rahola, J. E. Trinidad-Segovia, and F. J. de Las Nieves, Stock markets: A view from soft matter, *Physical Review E* **101**, 032307 (2020).
- [39] R. Cont, Empirical properties of asset returns: stylized facts and statistical issues, *Quantitative Finance* **1**, 223 (2001).
- [40] S. J. Kon, Models of stock returns—a comparison, *The Journal of Finance* **39**, 147 (1984).
- [41] H. Coronel-Brizio and A. Hernandez-Montoya, On fitting the pareto-levy distribution to stock market index data: Selecting a suitable cutoff value, *Physica A: Statistical Mechanics and its Applications* **354**, 437 (2005).
- [42] L. Kullmann, J. Töyli, J. Kertesz, A. Kanto, and K. Kaski, Characteristic times in stock market indices, *Physica A: Statistical Mechanics and its Applications* **269**, 98 (1999).
- [43] R. N. Mantegna and H. E. Stanley, Scaling behaviour in the dynamics of an economic index, *Nature* **376**, 46 (1995).
- [44] C. Borghesi, M. Marsili, and S. Micciche, Emergence of time-horizon invariant correlation structure in financial returns by subtraction of the market mode, *Physical Review E* **76**, 026104 (2007).
- [45] Y. Shapira, D. Y. Kenett, and E. Ben-Jacob, The index cohesive effect on stock market correlations, *The European Physical Journal B* **72**, 657 (2009).
- [46] A. Chakraborti, I. M. Toke, M. Patriarca, and F. Abergel, Econophysics review: I. empirical facts, *Quantitative Finance* **11**, 991 (2011).
- [47] S. Devi, Financial market dynamics: superdiffusive or not?, *Journal of Statistical Mechanics: Theory and Experiment* **2017**, 083207 (2017).
- [48] R. Cont, Volatility clustering in financial markets: empirical facts and agent-based models, in *Long memory in economics* (Springer, 2007) pp. 289–309.
- [49] V. Plerou and H. E. Stanley, Stock return distributions: tests of scaling and universality from three distinct stock markets, *Physical Review E* **77**, 037101 (2008).
- [50] M. Loretan and P. C. Phillips, Testing the covariance stationarity of heavy-tailed time series: An overview of the theory with applications to several financial datasets, *Journal of Empirical Finance* **1**, 211 (1994).
- [51] P. Gopikrishnan, V. Plerou, L. A. N. Amaral, M. Meyer, and H. E. Stanley, Scaling of the distribution of fluctuations of financial market indices, *Physical Review E* **60**, 5305 (1999).

- [52] J.-P. Bouchaud, Power laws in economics and finance: some ideas from physics, *Quantitative Finance* **1**, 105 (2001).
- [53] T. Bollerslev, R. Y. Chou, and K. F. Kroner, Arch modeling in finance: A review of the theory and empirical evidence, *Journal of Econometrics* **52**, 5 (1992).
- [54] M. Baity-Jesi, L. Sagun, M. Geiger, S. Spigler, G. B. Arous, C. Cammarota, Y. LeCun, M. Wyart, and G. Biroli, Comparing dynamics: Deep neural networks versus glassy systems, in *International Conference on Machine Learning* (PMLR, 2018) pp. 314–323.
- [55] G. Chen, C. K. Qu, and P. Gong, Anomalous diffusion dynamics of learning in deep neural networks, *Neural Networks* **149**, 18 (2022).
- [56] W. A. Little, The existence of persistent states in the brain, *Mathematical Biosciences* **19**, 101 (1974).
- [57] E. Gardner and B. Derrida, Three unfinished works on the optimal storage capacity of networks, *Journal of Physics A: Mathematical and General* **22**, 1983 (1989).
- [58] Y. Shi, C. L. Porter, J. C. Crocker, and D. H. Reich, Dissecting fat-tailed fluctuations in the cytoskeleton with active micropost arrays, *Proceedings of the National Academy of Sciences* **116**, 13839 (2019).
- [59] Y. Shi, S. Sivarajan, K. M. Xiang, G. M. Kostecki, L. Tung, J. C. Crocker, and D. H. Reich, Pervasive cytoquakes in the actomyosin cortex across cell types and substrate stiffness, *Integrative Biology* **13**, 246 (2021).
- [60] Y. LeCun, Y. Bengio, and G. Hinton, Deep learning, *nature* **521**, 436 (2015).